scientific reports

Check for updates

OPEN

Impact of the sequence of system-environment interactions on the functionality and efficiency of quantum thermal machines

Rui Huang[1,2], Zhong-Xiao Man[1,2✉], Lu Li[1] & Yun-Jie Xia[1]

In this work, we investigate effects of the sequence of system-environment interactions on the functionality and performance of quantum thermal machines (QTMs). The working substance of our setup consists of two subsystems, each independently coupled to its local thermal reservoir and further interconnected with a common reservoir in a cascaded manner. We demonstrate the impact of the sequential interactions between the subsystems and the common reservoir by exchanging the temperatures of the two local reservoirs. Our findings reveal that, when the two subsystems are in resonance, such an exchange alters the efficiency of QTMs without changing their functional types. Conversely, when the two subsystems are detuned, this exchange not only changes the efficiency but also the types of QTMs. Our results indicate that the manners of system-reservoir interactions offer significant potential for designing QTMs with tailored functionalities and enhanced performance.

Keywords Quantum thermodynamics, Quantum thermal machine, Cascaded model, Collision model

With the progress in quantum information science and technology, it has become increasingly clear that quantum mechanics offers unique resources and effects that allow for the achievement of tasks that are unattainable through classical resources and traditional approaches[1]. Consequently, the extension of the benefits of quantum resources and effects into various traditional domains has become as a crucial and pertinent topic. In this regard, quantum thermodynamics, which integrates classical thermodynamics with quantum mechanics, has garnered significant attention[2–7]. One of its primary goals is to explore the application of quantum tools in the design of quantum thermal machines (QTMs)[8–10], thereby demonstrating the quantum superiority within the realm of thermodynamics.

The operating prototype of the QTM was first conceptualized by Scovil and Schultz-Dubois[11], paving the way for subsequent proposals of a multitude of QTM models. QTMs adopt quantum systems as their working material to accomplish thermodynamic tasks through interaction with thermal baths at different temperatures, occasionally with the assistance of external power sources. In general, QTMs can be classified into two categories: stroke-based and continuous ones. Stroke-based QTMs encompass several independent heat and power processes, such as traditional Otto and Carnot cycles[12–22], as well as simplified versions that operate with just two strokes[23,24]. On the other hand, in continuous QTMs, the working material remains continually coupled with thermal baths to perform thermodynamic tasks[25–27]. One of the primary ways to utilize quantum resources and effects in actual QTMs is to incorporate them into the working substance[28–40]. Research has demonstrated that the quantum refrigerator comprising just three qubits can surpass its classical counterpart in terms of cooling efficiency and energy transfer, thanks to the entanglement of these qubits[28]. Furthermore, quantum engines employing two coupled qubits to execute a generalized Otto cycle exhibit a link between the work produced and the qubits' correlations[29]. Experimental results also support the superiority of quantum resources in powering quantum engines, exemplified by the utilization of nitrogen vacancy centers in diamond[41] and a spin-1/2 system with nuclear magnetic resonance techniques[32].

In comparison to QTMs operating on a stroke-based mechanism, the continuous QTMs avoid the need for stroke transformations, resulting in a simpler design, which is also the focus of this work. A paradigmatic illustration of continuous QTM consists of coupled systems interacting at their boundaries with two reservoirs of different temperatures, which is also referred to as boundary-driven QTMs[42–47]. If the internal interaction of the system cannot satisfy energy conservation, the involvement of external work source is necessary, enabling

[1]School of Physics and Physical Engineering, Qufu Normal University, Qufu 273165, China. [2]Rui Huang and Zhong-Xiao Man contributed equally to this work. ✉email: zxman@qfnu.edu.cn

it to function as an engine, refrigerator, or accelerator[42]. This boundary-driven two-reservoir model has been extended to the situation with three reservoirs, where an extra common reservoir is introduced for the whole system apart from the two local ones[48–51]. It turns out that due to the unique quantum effects brought about by the common reservoir, QTMs can achieve additional functionalities and experience performance enhancements. It shows that the machine can operate in otherwise forbidden regimes in the presence of a common non-equilibrium reservoir with coherence[50]. By considering a bipartite system coupled to both independent and common reservoirs, the effects of different types of system-reservoir interactions on work costs are unveiled and the operating regimes of QTMs are manifested[51].

In addition to simultaneous interactions with a common reservoir, subsystems of a multipartite system can interact with the reservoir sequentially, a configuration known as the cascade model[52–55]. The impact of cascaded model on QTMs is an issue worthy of exploration. The cascaded model illustrates a scenario where subsystems, specifically S_1 and S_2, successively interact with a reservoir in such a way that S_1 interacts with it at first, followed by S_2, resulting in a unidirectional influence from S_1 to S_2. This model possesses an inherent temporal structure, enabling it to delineate the sequential interactions between subsystems and the reservoir. For example, in a linear arrangement of QED cavities, information (or energy) can be exchanged unidirectionally through the successive passage of injected atoms through each cavity. The question of how cascaded interactions impact the functionality and performance of QTMs, in contrast to simultaneous interactions, remains unresolved. In this study, we investigate a QTM composed of two subsystems, each coupled to its own local reservoir and, concurrently, interacting with a third reservoir in a cascaded fashion. For comparative analysis, we also explore the scenario where the two subsystems interact simultaneously with the third reservoir. Our primary focus is on the operational regimes attainable through these models, with an aim to identify configurations that could potentially enhance the performance of QTMs.

The model and master equation

Our system $\mathcal{S}$ consists of two subsystems S_1 and S_2 being coupled locally to their own reservoirs R_A and R_B, respectively. The two subsystems are bridged by the third reservoir R_C, with which they interact together (cf. Fig.1a). Within the framework of collision model[56–64], the reservoir R_C is simulated as a collection of identically prepared ancillae with the generic Hamiltonian $\hat{H}_{R_C}$. The system interacts/collides with the ancillae one by one, with each collision lasting a short duration τ. After each collision, the ancilla is discarded, and the system collides with a new one in the next step of collision. The cascaded model (cf. Fig.1b) represents a unique type of collision model, wherein the subsystem S_1 collides firstly with an ancilla, followed by S_2 colliding with the same ancilla. Consequently, the dynamics of S_1 exert an influence on S_2, but the reverse does not hold true. For comparison, we also consider the simultaneous interactions between the system, S_1 and S_2, and the ancilla (cf. Fig.1c).

To be specific, we assume that both the subsystems S_1 and S_2 and generic ancilla of the reservoir R_C are two-level systems with the Hamiltonians $\hat{H}_{S_1} = \omega_{S_1}\hat{\sigma}_{S_1}^z/2$, $\hat{H}_{S_2} = \omega_{S_2}\hat{\sigma}_{S_2}^z/2$ and $\hat{H}_{R_C} = \omega_C\hat{\sigma}_{R_C}^z/2$, respectively, in which ω_{S_1}, ω_{S_2} and ω_C are the corresponding frequencies and $\{\hat{\sigma}_{\mathcal{O}}^x, \hat{\sigma}_{\mathcal{O}}^y, \hat{\sigma}_{\mathcal{O}}^z\}$ the usual Pauli operators acting on $\mathcal{O}$. The local reservoirs R_A and R_B are considered to be Bosonic ones governed by $\hat{H}_{R_A} = \sum_k \omega_{A,k}\hat{a}_k^\dagger\hat{a}_k$ and $\hat{H}_{R_B} = \sum_j \omega_{B,j}\hat{b}_j^\dagger\hat{b}_j$, respectively, with $\omega_{A,k}$ ($\omega_{B,j}$) the frequency of mode k (j) of reservoir R_A (R_B), $\hat{a}_k^\dagger$ ($\hat{b}_j^\dagger$) and $\hat{a}_k$ ($\hat{b}_j$) are annihilation and generation operators of mode k (j). The local interactions of $S_1 - R_A$ and $S_2 - R_B$ are characterized by the Hamiltonians

$$\hat{H}_{S_1 R_A} = \sum_k g_{A,k}\left(\hat{\sigma}_1^+\hat{a}_k + \hat{\sigma}_1^-\hat{a}_k^\dagger\right),\tag{1}$$

and
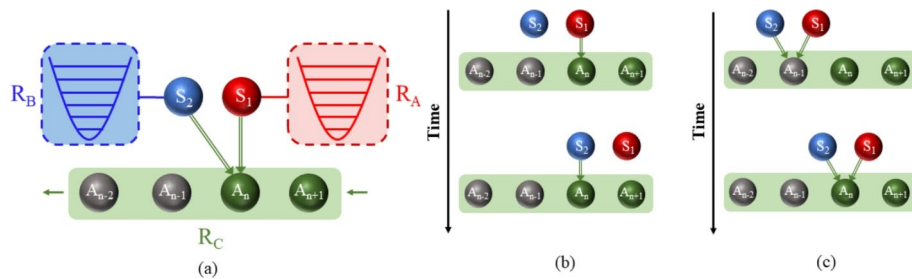
Fig. 1. (Color online) (**a**) Schematic diagram of our setup. The working substances S_1 and S_2 are locally coupled to the thermal reservoirs R_A and R_B, respectively, and meanwhile interact with the third reservoir R_C. Within the framework of collision model, the reservoir R_C is simulated by a collection of identically prepared ancillae. (**b**) Schematic diagram of the cascade model, where the subsystem S_1 interacts with a generic ancilla in R_C first, followed by the interaction of S_2 with the same ancilla. (**c**) Schematic diagram for the simultaneous interaction between S_1 and S_2 with a generic ancilla.

$$\hat{H}_{S_2 R_B} = \sum_j g_{B,j} \left(\hat{\sigma}_2^+ \hat{b}_j + \hat{\sigma}_2^- \hat{b}_j^\dagger \right), \tag{2}$$

with $g_{A,k}$ and $g_{B,j}$ the coupling strengths, and $\hat{\sigma}_1^+$ $(\hat{\sigma}_2^+)$ and $\hat{\sigma}_1^-$ $(\hat{\sigma}_2^-)$ the raising and lowering operators for the two-level subsystem S_1 (S_2), respectively.

The total Hamiltonian of the system plus reservoirs can be expressed as

$$\hat{H}_{tot}(t) = \hat{H}_S + \hat{H}_R + \hat{H}_{S_1 R_A} + \hat{H}_{S_2 R_B} + \sum_{i=1}^2 \lambda_i(t) \hat{V}_{int}^{(i)}, \tag{3}$$

where $\hat{H}_S = \sum_{i=1}^2 \hat{H}_{S_i}$, $\hat{H}_R = \sum_{l=A,B,C} \hat{H}_{R_l}$, and $\hat{V}_{int}^{(i)}$ is the interaction Hamiltonian of S_i with R_C. In Eq. (3), the step function $\lambda_i(t)$ represents the time-dependence of the collisions between the system and the reservoir R_C, which takes the value 1 when $t \in [(n-2+i)\tau, (n-1+i)\tau]$ with $n \geq 1$ the number of collisions, and zero otherwise. After a step of collision, the state ρ_S of the system at time t evolves to ρ_S' at time $t + 2\tau$ taking the form of

$$\rho_S' = \text{tr}_{R_C} \rho_{SR_C}' = \text{tr}_{R_C} \left\{ \hat{U}_2(\tau) \hat{U}_1(\tau) \rho_{SR_C} \hat{U}_1^\dagger(\tau) \hat{U}_2^\dagger(\tau) \right\}, \tag{4}$$

in which $\hat{U}_i(\tau) = e^{-i\tau(\hat{H}_{S_i} + \hat{H}_{R_C} + \hat{V}_{int}^{(i)})}$ is the unitary time evolution operator, $\rho_{SR_C} = \rho_S \otimes \rho_{R_C}^{th}$ and $\rho_{R_C}^{th} = e^{-\beta_C \hat{H}_{R_C}} / Z_{R_C}$ the initial thermal state of the reservoir R_C at inverse temperature $\beta_C = 1/T_C$ with $Z_{R_C} = \text{tr} \left\{ e^{-\beta_C \hat{H}_{R_C}} \right\}$ the partition function. We adopt $\hbar = k_B = 1$ here and throughout the paper.

The master equation that depicts the system's dynamics can be formulated as

$$\dot{\rho}_S = -i \left[\hat{H}_S, \rho_S \right] + \mathcal{L}_A(\rho_S) + \mathcal{L}_B(\rho_S) + \mathcal{L}_C(\rho_S) \tag{5}$$

where $\mathcal{L}_A$ and $\mathcal{L}_B$ denote the dissipations of the subsystems S_1 and S_2 due to the coupling with thermal reservoirs R_A and R_B, respectively, while $\mathcal{L}_C$ represents the dissipation of the system due to collisions with the intermediate reservoir R_C. In the above formula (5), the dissipative operators $\mathcal{L}_A(\rho_S)$ and $\mathcal{L}_B(\rho_S)$ are introduced phenomenologically, which can be expressed as

$$\begin{aligned} \mathcal{L}_A(\rho_S) =& \Gamma_A \left[\bar{n}_A(\omega_{S_1}) + 1 \right] \left(\hat{\sigma}_1^- \rho_S \hat{\sigma}_1^+ - \frac{1}{2} \left[\hat{\sigma}_1^+ \hat{\sigma}_1^-, \rho_S \right]_+ \right) \\ & + \Gamma_A \bar{n}_A(\omega_{S_1}) \left(\hat{\sigma}_1^+ \rho_S \hat{\sigma}_1^- - \frac{1}{2} \left[\hat{\sigma}_1^- \hat{\sigma}_1^+, \rho_S \right]_+ \right) \end{aligned} \tag{6}$$

and

$$\begin{aligned} \mathcal{L}_B(\rho_S) =& \Gamma_B \left[\bar{n}_B(\omega_{S_2}) + 1 \right] \left(\hat{\sigma}_2^- \rho_S \hat{\sigma}_2^+ - \frac{1}{2} \left[\hat{\sigma}_2^+ \hat{\sigma}_2^-, \rho_S \right]_+ \right) \\ & + \Gamma_B \bar{n}_B(\omega_{S_2}) \left(\hat{\sigma}_2^+ \rho_S \hat{\sigma}_2^- - \frac{1}{2} \left[\hat{\sigma}_2^- \hat{\sigma}_2^+, \rho_S \right]_+ \right), \end{aligned} \tag{7}$$

respectively. In Eqs. (6) and (7), Γ_A (Γ_B) denotes the damping rates of the reservoir R_A (R_B), and $\bar{n}_A(\omega_{S_1})$ $(\bar{n}_B(\omega_{S_2}))$ is the average number of photons of R_A (R_B) at the frequency ω_{S_1} (ω_{S_2}) of the subsystem S_1 (S_2) which takes the form

$$\bar{n}_l(\omega_{S_i}) = \frac{1}{\exp\left(\frac{\omega_{S_i}}{T_l}\right) - 1}. \tag{8}$$

By expanding $\hat{U}_i(\tau)$ to the second order of τ, we obtain the dissipative operator $\mathcal{L}_C(\rho_S)$, which can be decomposed into the following form

$$\mathcal{L}_C(\rho_S) = \sum_{i=1}^2 \mathcal{L}_i(\rho_S) + \mathcal{D}_{12}(\rho_S) \tag{9}$$

with

$$\mathcal{L}_i(\rho_S) = -\frac{1}{2} \text{tr}_{R_C} \left\{ \left[\hat{V}_{int}^{(i)}, \left[\hat{V}_{int}^{(i)}, \rho_S \otimes \rho_{R_C}^{th} \right] \right] \right\} \tag{10}$$

representing the local dissipation of S_i as if only S_i exists and

$$\mathcal{D}_{12}\left(\rho_S\right) = -\mathrm{tr}_{R_C}\left\{\left[\hat{V}_{int}^{(2)},\left[\hat{V}_{int}^{(1)},\rho_S\otimes\rho_{R_C}^{th}\right]\right]\right\} \tag{11}$$

characterizing the collective dissipation of the two subsystems due to their cascaded interactions with R_C. Here, the dissipator $\mathcal{D}_{12}$ incorporates the one-way influence between subsystems, which alternatively can also be manifested in a chiral effective Hamiltonian of the system[57].

In the following illustrations, the interactions between the subsystems S_1 and S_2 and the reservoir R_C are taken to be

$$\hat{V}_{int}^{(1)} = \frac{1}{\sqrt{\tau}}\left(J_1^x\hat{\sigma}_{S_1}^x\hat{\sigma}_{R_C}^x + J_1^y\hat{\sigma}_{S_1}^y\hat{\sigma}_{R_C}^y\right), \tag{12}$$

and

$$\hat{V}_{int}^{(2)} = \frac{1}{\sqrt{\tau}}\left(J_2^x\hat{\sigma}_{S_2}^x\hat{\sigma}_{R_C}^x + J_2^y\hat{\sigma}_{S_2}^y\hat{\sigma}_{R_C}^y\right), \tag{13}$$

respectively, in which the interactions have been scaled by the collision duration τ for the convenience of taking continuous time limit, although this is not strictly necessary. As a result, the local and non-local dissipations, given by Eqs.(10) and (11), can be updated to

$$\begin{aligned}
\mathcal{L}_i\left(\rho_S\right) = &(J_i^x)^2\left(\hat{\sigma}_{S_i}^x\rho_S\hat{\sigma}_{S_i}^x - \frac{1}{2}\left[\rho_S,\hat{\sigma}_{S_i}^x\hat{\sigma}_{S_i}^x\right]_+\right)\\
&+ (J_i^y)^2\left(\hat{\sigma}_{S_i}^y\rho_S\hat{\sigma}_{S_i}^y - \frac{1}{2}\left[\rho_S,\hat{\sigma}_{S_i}^y\hat{\sigma}_{S_i}^y\right]_+\right)\\
&- iJ_i^xJ_i^y\left\langle\hat{\sigma}_{R_C}^z\right\rangle_{\rho_{R_C}^{th}}\left[\left(\hat{\sigma}_{S_i}^x\rho_S\hat{\sigma}_{S_i}^y - \frac{1}{2}\left[\rho_S,\hat{\sigma}_{S_i}^y\hat{\sigma}_{S_i}^x\right]_+\right)\right.\\
&\left.- \left(\hat{\sigma}_{S_i}^y\rho_S\hat{\sigma}_{S_i}^x - \frac{1}{2}\left[\rho_S,\hat{\sigma}_{S_i}^x\hat{\sigma}_{S_i}^y\right]_+\right)\right],
\end{aligned} \tag{14}$$

and

$$\begin{aligned}
\mathcal{D}_{12}\left(\rho_S\right) = &i\left\langle\hat{\sigma}_{R_C}^z\right\rangle_{\rho_{R_C}^{th}}\left\{\left(J_1^xJ_2^y\left[\hat{\sigma}_{S_2}^y,\rho_S\hat{\sigma}_{S_1}^x\right] + J_1^yJ_2^x\left[\hat{\sigma}_{S_1}^y\rho_S,\hat{\sigma}_{S_2}^x\right]\right)\right.\\
&\left.- \left(J_1^yJ_2^x\left[\hat{\sigma}_{S_2}^x,\rho_S\hat{\sigma}_{S_1}^y\right] + J_1^xJ_2^y\left[\hat{\sigma}_{S_1}^x\rho_S,\hat{\sigma}_{S_2}^y\right]\right)\right\}\\
&+ J_1^xJ_2^x\left[\hat{\sigma}_{S_2}^x,\left[\rho_S,\hat{\sigma}_{S_1}^x\right]\right] + J_1^yJ_2^y\left[\hat{\sigma}_{S_2}^y,\left[\rho_S,\hat{\sigma}_{S_1}^y\right]\right],
\end{aligned} \tag{15}$$

with $\langle\cdot\rangle_\rho \equiv \mathrm{tr}[\cdot\rho]$.

To compare the cascaded interaction with simultaneous interaction between the two subsystems and the reservoir R_C, we also present the master equation for the latter case. For the simultaneous interaction, the structure of local dissipation remains the same as that given in Eq. (10), while the non-local dissipation can be expressed as

$$\begin{aligned}
\mathcal{D}_{12}^{sim}\left(\rho_S\right) = &-\frac{1}{2}\mathrm{tr}_{R_C}\left[\hat{V}_{int}^{(1)},\left[\hat{V}_{int}^{(2)},\rho_S\otimes\rho_{R_C}^{th}\right]\right]\\
&-\frac{1}{2}\mathrm{tr}_{R_C}\left[\hat{V}_{int}^{(2)},\left[\hat{V}_{int}^{(1)},\rho_S\otimes\rho_{R_C}^{th}\right]\right].
\end{aligned} \tag{16}$$

The non-local dissipation term of the simultaneous collision is more "symmetric" in comparison to the situation of cascaded collision. Taking into account the specific forms of interactions as given in Eqs. (12) and (13), the non-local dissipation can be expressed as

$$\begin{aligned}
\mathcal{D}_{12}^{sim}\left(\rho_S\right) = &\frac{i}{2}\left\langle\hat{\sigma}_{R_C}^z\right\rangle_{\rho_{R_C}^{th}}\left(J_1^xJ_2^y\left(\left[\hat{\sigma}_{S_2}^y,\rho_S\hat{\sigma}_{S_1}^x\right] + \left[\hat{\sigma}_{S_2}^y\rho_S,\hat{\sigma}_{S_1}^x\right]\right)\right.\\
&\left.+ J_1^yJ_2^x\left(\left[\hat{\sigma}_{S_1}^y\rho_S,\hat{\sigma}_{S_2}^x\right] + \left[\hat{\sigma}_{S_1}^y,\rho_S\hat{\sigma}_{S_2}^x\right]\right)\right)\\
&-\frac{i}{2}\left\langle\hat{\sigma}_{R_C}^z\right\rangle_{\rho_{R_C}^{th}}\left(J_1^yJ_2^x\left(\left[\hat{\sigma}_{S_2}^x,\rho_S\hat{\sigma}_{S_1}^y\right] + \left[\hat{\sigma}_{S_2}^x\rho_S,\hat{\sigma}_{S_1}^y\right]\right)\right.\\
&\left.+ J_1^xJ_2^y\left(\left[\hat{\sigma}_{S_1}^x\rho_S,\hat{\sigma}_{S_2}^y\right] + \left[\hat{\sigma}_{S_1}^x,\rho_S\hat{\sigma}_{S_2}^y\right]\right)\right)\\
&+\frac{J_1^xJ_2^x}{2}\left(\left[\hat{\sigma}_{S_1}^x\left[\rho_S,\hat{\sigma}_{S_2}^x\right]\right] + \left[\hat{\sigma}_{S_2}^x\left[\rho_S,\hat{\sigma}_{S_1}^x\right]\right]\right)\\
&+\frac{J_1^yJ_2^y}{2}\left(\left[\hat{\sigma}_{S_1}^y\left[\rho_S,\hat{\sigma}_{S_2}^y\right]\right] + \left[\hat{\sigma}_{S_2}^y\left[\rho_S,\hat{\sigma}_{S_1}^y\right]\right]\right).
\end{aligned} \tag{17}$$

Thermodynamic quantities

The heat currents from the reservoirs R_A and R_B to the system can be defined as the energy change of the system due to the dissipations of the reservoirs, which are formulated as $J_A = \mathrm{Tr} \left\{ \mathcal{L}_A \left[\rho_S \right] \hat{H}_{S_1} \right\}$ and $J_B = \mathrm{Tr} \left\{ \mathcal{L}_B \left[\rho_S \right] \hat{H}_{S_2} \right\}$, respectively. For the dissipations given in Eqs. (6) and (7), we can obtain the explicit forms of heat currents as

$$J_A = \Gamma_A \omega_{S_1} \left(n_A \left\langle \hat{\sigma}_{S_1}^- \hat{\sigma}_{S_1}^+ \right\rangle_{\rho_S} - (n_A + 1) \left\langle \hat{\sigma}_{S_1}^+ \hat{\sigma}_{S_1}^- \right\rangle_{\rho_S} \right), \tag{18}$$

and

$$J_B = \Gamma_B \omega_{S_2} \left(n_B \left\langle \hat{\sigma}_{S_2}^- \hat{\sigma}_{S_2}^+ \right\rangle_{\rho_S} - (n_B + 1) \left\langle \hat{\sigma}_{S_2}^+ \hat{\sigma}_{S_2}^- \right\rangle_{\rho_S} \right), \tag{19}$$

in which $n_A \equiv \bar{n}_A(\omega_{S_1})$ and $n_B \equiv \bar{n}_B(\omega_{S_2})$.

The heat transferred from the middle reservoir R_C to the system can be quantified by the energy variations of R_C during a collision as

$$\Delta J_C = -\mathrm{tr} \left\{ \hat{H}_{R_C} \left(\rho'_{SR_C} - \rho_{SR_C} \right) \right\}. \tag{20}$$

We note that due to the collective interaction between R_C and the two subsystems S_1 and S_2, the heat can be decomposed into the local component $\Delta J_C^{(i)}$ associated with S_i and nonlocal one $\Delta J_C^{(12)}$ related to the nonlocal dissipation of R_C, that is, $\Delta J_C = \sum_{i=1}^{2} \Delta J_C^{(i)} + \Delta J_C^{(12)}$. By taking the continuous time limit, we get the heat current as

$$J_C = -\lim_{\tau \to 0} \frac{\Delta J_C}{\tau} = \sum_{i=1}^{2} J_C^{(i)} + J_C^{(12)}. \tag{21}$$

According to the map given in Eq. (4), the local and nonlocal components of heat current J_C can be derived as

$$J_C^{(i)} = \frac{1}{2} \mathrm{tr} \left\{ \left[\hat{V}_{int}^{(i)}, \left[\hat{H}_{R_C}, \hat{V}_{int}^{(i)} \right] \right] \rho_{SR_C} \right\} \tag{22}$$

and

$$J_C^{(12)} = \mathrm{tr} \left\{ \left[\hat{V}_{int}^{(1)}, \left[\hat{H}_{R_C}, \hat{V}_{int}^{(2)} \right] \right] \rho_{SR_C} \right\}, \tag{23}$$

respectively. For the specific interaction form shown in Eqs. (12) and (13), $J_C^{(i)}$ and $J_C^{(12)}$ can be further expressed as

$$J_C^{(i)} = -\omega_C \left[2 J_i^x J_i^y \left\langle \sigma_{S_i}^z \right\rangle_{\rho_S} - \left((J_i^x)^2 + (J_i^y)^2 \right) \left\langle \sigma_{R_C}^z \right\rangle_{\rho_{R_C}^{th}} \right], \tag{24}$$

and

$$J_C^{(12)} = 2\omega_C \left\langle \sigma_{R_C}^z \right\rangle_{\rho_{R_C}^{th}} \left(J_1^x J_2^x \left\langle \sigma_{S_1}^x \sigma_{S_2}^x \right\rangle_{\rho_S} + J_1^y J_2^y \left\langle \sigma_{S_1}^y \sigma_{S_2}^y \right\rangle_{\rho_S} \right), \tag{25}$$

respectively.

Work in quantum thermodynamics is commonly defined as the alteration in energy of the total system resulting from time-variation of the Hamiltonian. Within the framework of collision model, the sequential couplings and decouplings of the system with the reservoir R_C give rise to the temporal dependence of the interaction Hamiltonian, as given in Eq.(3). Consequently, the energetic cost required to maintain these consecutive collisions is supplied in the form of work. In a round of collision from t to $t + 2\tau$, the work performed on the system is formulated as

$$\Delta W = \int_t^{t+2\tau} \left\langle \frac{\partial \hat{H}_{tot}(s)}{\partial s} \right\rangle_{\rho_{SR_C}} ds. \tag{26}$$

From the Hamiltonian $\hat{H}_{tot}(s)$, Eq. (3), we can see that only the interactions of the two subsystems with the reservoir R_C are time-dependent. After taking the continuous time limit, we can obtain the work current $\dot{W} = \lim_{\tau \to 0} \Delta W / \tau$. An integration over Eq. (26) yields

$$\dot{W} = \sum_{i=1}^{2} \dot{W}_i + \dot{W}_{12}, \tag{27}$$

with

$$\dot{W}_i = \frac{1}{2} \operatorname{tr} \left\{ \left[\hat{V}_{int}^{(i)}, \left[\hat{H}_{S_i} + \hat{H}_{R_C}, \hat{V}_{int}^{(i)} \right] \right] \rho_{SR_C} \right\}, \tag{28}$$

and

$$\dot{W}_{12} = \operatorname{tr} \left\{ \left[\hat{V}_{int}^{(1)}, \left[\hat{H}_{S_2} + \hat{H}_{R_C}, \hat{V}_{int}^{(2)} \right] \right] \rho_{SR_C} \right\}, \tag{29}$$

being the local and nonlocal components of the work current. Eq. (28) indicates that if $[\hat{H}_{S_i} + \hat{H}_{R_C}, \hat{V}_{int}^{(i)}] = 0$, namely, the interaction between the subsystem S_i and the reservoir R_C conserves energy, the local work current $\dot{W}_i$ vanish. Moreover, when the local work current $\dot{W}_2$ is zero, the non-local work current $\dot{W}_{12}$ must also be zero. However, as can be seen from the subsequent formula (31), $\dot{W}_{12}$ also depend on the correlations established between S_1 and S_2. Even if W_2 is not zero, the absence of correlations between S_1 and S_2 in terms of $\langle \sigma_{S_1}^x \sigma_{S_2}^x \rangle_{\rho_S}$ and $\langle \sigma_{S_1}^y \sigma_{S_2}^y \rangle_{\rho_S}$ will also lead to the disappearance of $\dot{W}_{12}$. For the specific interactions given in Eqs. (12) and (13), the local work current reads

$$\begin{aligned}
\dot{W}_i =& \omega_{S_i} \left(2J_i^x J_i^y \langle \sigma_{R_C}^z \rangle_{\rho_{R_C}^{th}} - \left((J_i^x)^2 + (J_i^y)^2 \right) \langle \sigma_{S_i}^z \rangle_{\rho_S} \right) \\
&+ \omega_C \left(2J_i^x J_i^y \langle \sigma_{S_i}^z \rangle_{\rho_S} - \left((J_i^x)^2 + (J_i^y)^2 \right) \langle \sigma_{R_C}^z \rangle_{\rho_{R_C}^{th}} \right),
\end{aligned} \tag{30}$$

while the nonlocal component can be expressed as

$$\begin{aligned}
\dot{W}_{12} =& 2J_1^x \left(\omega_{S_2} J_2^y - \omega_C J_2^x \right) \langle \sigma_{S_1}^x \sigma_{S_2}^x \rangle_{\rho_S} \langle \sigma_{R_C}^z \rangle_{\rho_{R_C}^{th}} \\
&+ J_1^y \left(\omega_{S_2} J_2^x - \omega_C J_2^y \right) \langle \sigma_{S_1}^y \sigma_{S_2}^y \rangle_{\rho_S} \langle \sigma_{R_C}^z \rangle_{\rho_{R_C}^{th}}.
\end{aligned} \tag{31}$$

Here, we also derive the work current regarding the simultaneous interactions between the subsystems and reservoir R_C. Since the local component of the work current for the simultaneous interactions is the same as that given in Eqs. (28) and (30) for the cascaded interactions, we only present its general nonlocal component as

$$\begin{aligned}
\dot{W}_{12}^{\text{sim}} =& \frac{1}{2} \operatorname{tr} \left\{ \left[\hat{V}_{\text{int}}^{(1)}, \left[\hat{H}_{S_2} + \hat{H}_{R_C}, \hat{V}_{\text{int}}^{(2)} \right] \right] \rho_{SR_C} \right\} \\
&+ \frac{1}{2} \operatorname{tr} \left\{ \left[\hat{V}_{\text{int}}^{(2)}, \left[\hat{H}_{S_1} + \hat{H}_{R_C}, \hat{V}_{\text{int}}^{(1)} \right] \right] \rho_{SR_C} \right\},
\end{aligned} \tag{32}$$

and the specific form as

$$\begin{aligned}
\dot{W}_{12}^{\text{sim}} =& J_1^x \left(\omega_{S_2} J_2^y - \omega_C J_2^x \right) \langle \sigma_{S_1}^x \sigma_{S_2}^x \rangle_{\rho_S} \langle \sigma_{R_C}^z \rangle_{\rho_{R_C}^{th}} \\
&+ J_1^y \left(\omega_{S_2} J_2^x - \omega_C J_2^y \right) \langle \sigma_{S_1}^y \sigma_{S_2}^y \rangle_{\rho_S} \langle \sigma_{R_C}^z \rangle_{\rho_{R_C}^{th}} \\
&+ J_2^x \left(\omega_{S_1} J_1^y - \omega_C J_1^x \right) \langle \sigma_{S_2}^x \sigma_{S_1}^x \rangle_{\rho_S} \langle \sigma_{R_C}^z \rangle_{\rho_{R_C}^{th}} \\
&+ J_2^y \left(\omega_{S_1} J_1^x - \omega_C J_1^y \right) \langle \sigma_{S_2}^y \sigma_{S_1}^y \rangle_{\rho_S} \langle \sigma_{R_C}^z \rangle_{\rho_{R_C}^{th}}.
\end{aligned} \tag{33}$$

Quantum thermal machines

After properly defining thermodynamic quantities, we are ready to study the functions that our setup can achieve as QTMs, as well as their performance in different scenarios. In the following, we mainly examine two configurations: one is the symmetric case where two subsystems S_1 and S_2 are resonant, and the other is the asymmetric case with detuning between them. We unveil different functions exhibited by the system relying on variations of the frequency of ancillas in the reservoir R_C.

Symmetric case

In order to obtain explicit operating regimes for the system, we first consider a specific situation, namely, $\omega_{S_1} = \omega_{S_2}$, $J_1^x = J_1^y = J_2^x = J_2^y = J$. In this case, we find the system can achieve four different functions within certain ranges of the frequency ω_C of the reservoir R_C, as shown in the Table 1. As the temperatures of the three reservoirs are not determined in prior, we have used $\dot{Q}_h$ and $\dot{Q}_c$ to represent the heat currents for reservoirs with the highest and the coldest temperatures, and $\dot{Q}_m$ for the reservoir with middle temperature. In

Label	Description	$\dot{Q}_c$	$\dot{Q}_m$	$\dot{Q}_h$	$\dot{W}$
I	T_C-power driven refrigerator	< 0	> 0	< 0	> 0
II	Dual-source accelerator	< 0	> 0	> 0	> 0
III	Dual-source engine	< 0	> 0	> 0	< 0
IV	Dual-sink accelerator	< 0	< 0	> 0	> 0

Table 1. Table of operating regimes of the machine for the symmetric case with $\omega_{S_1} = \omega_{S_2}$. The first column shows the labels of different regimes; the second column describes the functions and features of the machine; the remaining columns give the signs of the heat and work currents.
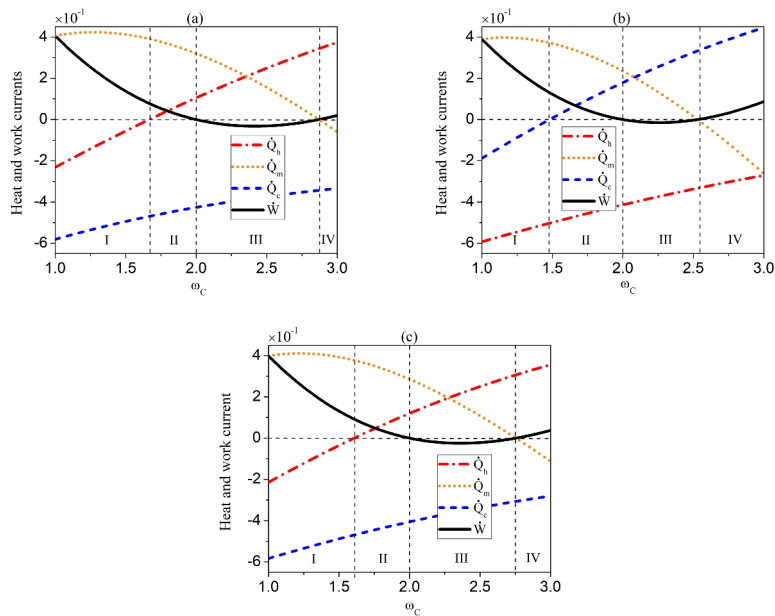
Fig. 2. (Color online) The currents of heat and work as a function of the frequency ω_C of ancilla of the reservoir R_C for the symmetric case. The cascaded interactions between subsystems S_1 and S_2 and R_C for $T_A = 2.4\omega_C > T_C = 2\omega_C > T_B = 0.5\omega_C$ (**a**) and $T_A = 0.5\omega_C < T_C = 2\omega_C < T_B = 2.4\omega_C$ (**b**). The simultaneous interactions between S_1 and S_2 and R_C (**c**). The other parameters are chosen as $\omega_{S_1} = \omega_{S_2} = 2\omega_C, J = \omega_C, \Gamma_A = \Gamma_B = 1$.

the following, we shall consider two settings of the temperatures, namely, $T_A > T_C > T_B$ and $T_A < T_C < T_B$, with the temperature of reservoir R_C always being the intermediate one.

We first consider the case of $T_A > T_C > T_B$, for which $\dot{Q}_h \equiv J_A$, $\dot{Q}_c \equiv J_B$, and $\dot{Q}_m \equiv J_C$. For the operating regime of Type I, namely, $\dot{W} > 0$, $\dot{Q}_m > 0$ and $\dot{Q}_h < 0$, the external agent performs work on the system, driving heat flow from the reservoir R_C with middle temperature to R_A with the highest temperature. Hence, the machine of Type I realizes the cooling of reservoir R_C, which is thus called the T_C-power driven-refrigerator. In the regime of Type II, apart from the external work on the system with $\dot{W} > 0$, the heat is transferred from the reservoirs R_A and R_C with relatively high temperatures to the reservoir R_B with relatively low temperature with $\dot{Q}_m > 0$, $\dot{Q}_h > 0$ and $\dot{Q}_c < 0$. Therefore, the machine of Type II operates as the dual-source accelerator (oven)[65] by acquiring external work and transporting heat from the dual sources R_A and R_C to R_B. The machine of Type III with $\dot{W} < 0$, $\dot{Q}_m > 0$, $\dot{Q}_h > 0$ and $\dot{Q}_c < 0$ obviously implements the dual-source engine, which perform work to an external agent by transferring heat from the reservoirs R_C and R_A to R_B. The Type IV of QTMs is also an accelerator, but unlike the Type II, it absorbs heat from the high-temperature reservoir R_A and dumps the heat into two relatively cooler reservoirs R_B and R_C, which is thus called dual-sink accelerator. In Fig. 2a, we plot the work current $\dot{W}$ and the three heat currents $\dot{Q}_m, \dot{Q}_h$ and $\dot{Q}_c$ with respect to the frequency ω_C of the ancilla of reservoir R_C. We have labeled the regions for appearances of different operating regimes according to the Table 1.

By reversing the temperatures of R_A and R_B to be $T_A < T_C < T_B$, we can still obtain the same four types of operating regimes as the case of $T_A > T_C > T_B$. However, the ranges in which these operating regimes appear are altered, as shown in Fig. 2b. This reflects the asymmetric characteristic of the cascaded interactions occurring between subsystems S_1 and S_2 with R_C.

In order to compare the cascaded interaction with simultaneous interaction, we illustrate the heat and work currents under the latter case in Fig. 2c. We can see that the simultaneous interaction does not change the types of QTMs compared to the cascaded interaction, but shifts the intervals of their occurrences. Moreover, if the
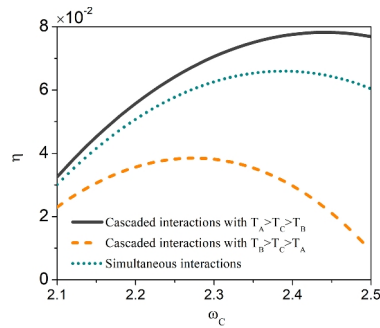
Fig. 3. (Color online) The efficiency of dual-source engine under three situations, i.e., the cascaded interactions between the two subsystems and the reservoir R_C with $T_A > T_B > T_C$ and $T_A < T_B < T_C$, and the simultaneous interactions. The other parameters are the same as that used in Fig. 2.

Label	Description	$\dot{Q}_c$	$\dot{Q}_m$	$\dot{Q}_h$	$\dot{W}$
I	T_C-power driven refrigerator	< 0	> 0	< 0	> 0
III	Dual-source engine	< 0	> 0	> 0	< 0
V	T_C-heat-driven refrigerator with work production	< 0	> 0	< 0	< 0
VI	Dual-sink engine	< 0	< 0	> 0	< 0

Table 2. Table of operating regimes of the machine for asymmetric case with $\omega_{S_1} \neq \omega_{S_2}$. The first column shows the labels of different regimes; the second column describes the functions and characters of the machine; the remaining columns give the signs of heat and work currents.

temperatures of the reservoirs R_A and R_B are reversed, there will be no influence on the results due to the symmetry character of the simultaneous interaction.

Next, we demonstrate the influences of different configurations, namely, the cascaded interaction with $T_A > T_C > T_B$ and $T_A < T_C < T_B$ as well as the simultaneous interaction, on the performance of QTMs. Here, we focus on the dual-source engine, which appears in the common interval $\omega_C \in (2.1, 2.5)$ for all these three situations. We use the efficiency to assess the performance of quantum engine, which can be defined as

$$\eta = \frac{\left|\dot{W}\right|}{\dot{Q}_h + \dot{Q}_m}. \tag{34}$$

We exhibit in Fig. 3 the efficiency η of dual-source engine with respect to ω_C for the three situations, i.e., the cascaded interaction with $T_A > T_C > T_B$ and $T_A < T_C < T_B$ and the simultaneous interaction. We observe that the cascaded interaction for the temperature setting $T_A > T_C > T_B$ can lead to the largest efficiency, while the configuration $T_A < T_C < T_B$ causes the lowest efficiency. The efficiency of simultaneous interaction is always in between these two cases.

Asymmetric case

In the following, we further consider the operating modes of our setup under the asymmetric situation where the two subsystems exhibit different frequencies, namely, $\omega_{S_1} \neq \omega_{S_2}$. For the interactions between the subsystems and the reservoir R_C, we still assume $J_1^x = J_1^y = J_2^x = J_2^y = J$. The results are presented in Table 2, which shows that apart from the Types I and III that have been achieved in the symmetric case, as shown in Table 1, two new types of thermal machines, i.e., Type V and Type VI, arise. For the QTM of Type V, called T_C-heat-driven refrigerator with work production, the heat current is transferred from the reservoir with an intermediate temperature to the reservoir with the highest temperature, functioning as a refrigerator, and at the same time the work is produced instead of being consumed. In the case of Type VI, the system perform work on an external agent by absorbing heat from the hot reservoir and releasing it to two other reservoirs, which is thus called dual-sink engine.

In Fig. 4a, we illustrate the operating regimes of the machines by plotting the work and heat currents against ω_C for the cascaded interactions with $T_A > T_C > T_B$, for which there appear three functions of the machines. In Fig. 4b, we exhibit the results by reversing the temperatures of R_A and R_B to be $T_A < T_C < T_B$ and meanwhile exchanging the positions of the two subsystems, which shows that all the four operating regimes listed in Table 2 can be observed. Therefore, the system manifests different functions in these two scenarios embodying the unidirectional feature of the cascaded interaction. Fig. 4c displays the case of simultaneous interaction of S_1 and S_2 with R_C, from which we can see that three types of machines arise, similar to that exhibited in Fig. 4a, but with different intervals.

8
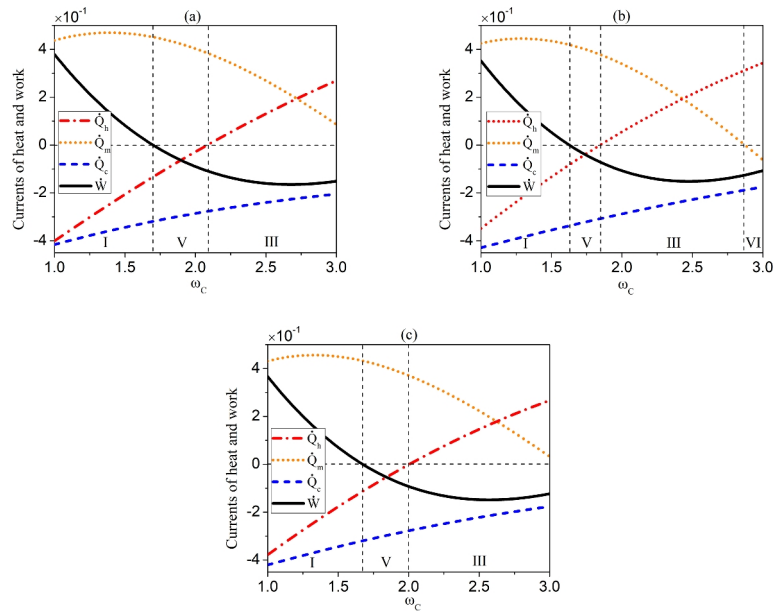
Fig. 4. (Color online) The currents of heat and work as a function of the frequency ω_C of ancilla of the reservoir R_C for the asymmetric case. The cascaded interactions between subsystems S_1 and S_2 and R_C for $T_A = 2.4\omega_C > T_C = 2\omega_C > T_B = 0.5\omega_C$ and $\omega_{S_1} = 2.5\omega_C$, $\omega_{S_2} = 1.5\omega_C$ (**a**), and $T_A = 0.5\omega_C < T_C = 2\omega_C < T_B = 2.4\omega_C$ and $\omega_{S_1} = 1.5\omega_C$, $\omega_{S_2} = 2.5\omega_C$ (**b**). The simultaneous interactions between S_1 and S_2 and R_C (**c**). The other parameter is the same as that used in Fig. 2.
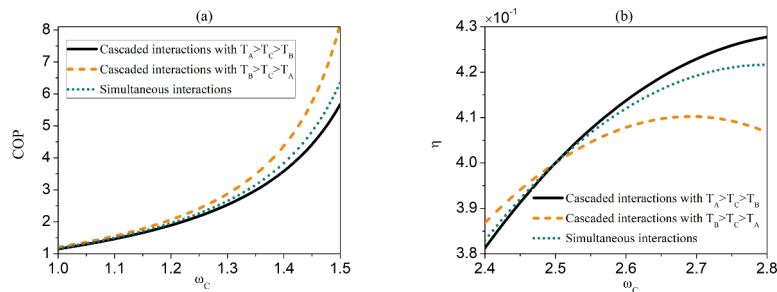
Fig. 5. (Color online) The COP of the T_C-power driven refrigerator (**a**) and the efficiency η of the dual-sink engine versus ω_C. The parameters are the same as that used in Fig.4.

Next, we compare the efficiency of the machines under different configurations by focusing on Type I (i.e., T_C-power driven refrigerator) and Type III (i.e., dual-source engine) of the machines. The coefficient of performance (COP) of a refrigerator is defined as

$$COP = \frac{\dot{Q}_c}{\dot{W}},\tag{35}$$

while the efficiency of the dual-sink engine is still quantified by the formula Eq. (34). In Fig. 5a and b, we show the COP of T_C-power driven refrigerator and the efficiency of dual-source engine as a function of ω_C for different situations. From Fig. 5a, we observe that the COP of the refrigerator for cascaded interaction entailing $T_B > T_C > T_A$ achieves the highest efficiency, while that with temperature $T_A > T_C > T_B$ has the lowest efficiency. The COP of refrigerator under simultaneous interaction falls between the two. From Fig. 5b, it can be seen that the efficiency of the engine relies on ω_C: for relatively small values of ω_C, the cascaded interaction with the temperature setting $T_B > T_C > T_A$ results in the highest efficiency, while for relatively large ω_C, the cascaded interaction with $T_A > T_C > T_B$ leads to the highest efficiency. The efficiency under the simultaneous interaction always falls between the two.

Conclusion
In conclusion, we have studied the impacts of the sequence of system-environment interactions on the operating regimes and performance of QTMs. The working substance of our setup consists of two subsystems, S_1 and S_2

, coupled to their local reservoirs R_A and R_B, respectively, and meanwhile to the third reservoir R_C through sequential interactions. For comparison, we have also considered the situation that the two subsystems interact simultaneously with R_C. Our findings indicate that the unidirectionality resulting from the sequential interaction between the subsystems and the reservoir R_C can influence both the functions and performance of QTMs. In the symmetric scenario where the two subsystems are resonant, although exchanging the temperatures of two local reservoirs R_A and R_B does not alter the functions of QTMs, such a swap significantly changes their efficiency: in one case, the efficiency surpasses that achieved when the system interacts simultaneously with the common reservoir R_C, whereas in another case, it falls below this level. In the antisymmetric scenario where the two subsystems are detuning, the exchange of R_A and R_B influences both the types of QTMs and their performance. Our results reveal the influence of the sequence of interactions between subsystems and the reservoir on the function and performance of QTMs, providing a potential means for their design and performance enhancement.

Data availability

The datasets used and/or analyzed during the current study are available from the corresponding author on reasonable request.

References

1. Nielsen, M. & Chuang, I. *Quantum Computation and Quantum Information* (Cambridge University Press, Cambridge, 2000).
2. Gemma, G., Michel, M. & Mahler, G. *Quantum Thermodynamics* (Springer, Berlin, 2004).
3. Deffner, S. & Campbell, S. *Quantum Thermodynamics: An introduction to the thermodynamics of quantum information*. 2053–2571 (Morgan and Claypool Publishers, 2019). https://doi.org/10.1088/2053-2571/ab21c6.
4. Kosloff, R. Quantum thermodynamics: A dynamical viewpoint. *Entropy* **15**, 2100. https://doi.org/10.3390/e15062100 (2013).
5. Vinjanampathy, S. & Anders, J. Quantum thermodynamics. *Contemp. Phys.* **57**, 545. https://doi.org/10.1080/00107514.2016.1201896 (2016).
6. Goold, J., Huber, M., Riera, A., del Rio, L. & Skrzypczyk, P. The role of quantum information in thermodynamics-a topical review. *J. Phys. A: Math. Theor.* **49**, 143001. https://doi.org/10.1088/1751-8113/49/14/143001 (2016).
7. Millen, J. & Xuereb, A. Perspective on quantum thermodynamics. *New J. Phys.* **18**, 011002. https://doi.org/10.1088/1367-2630/18/1/011002 (2016).
8. F. Binder, Correa, C. G. J. A. L. A. & Adesso, G. E. *Thermodynamics in the Quantum Regime. Fundamental Aspects and New Directions* (Springer, Switzerland, 2018).
9. Cangemi, L. M., Bhadra, C. & Levy, A. Quantum engines and refrigerators. *Phys. Rep.* **1087**, 1 (2024).
10. Mitchison, M. T. Quantum thermal absorption machines: Refrigerators, engines and clocks. *Contemp. Phys.* **60**, 164 (2019).
11. Scovil, H. E. D. & Schulz-DuBois, E. O. Three-level masers as heat engines. *Phys. Rev. Lett.* **2**, 262. https://doi.org/10.1103/PhysRevLett.2.262 (1959).
12. Quan, H. T., Liu, Y.-x, Sun, C. P. & Nori, F. Quantum thermodynamic cycles and quantum heat engines. *Phys. Rev. E* **76**, 031105. https://doi.org/10.1103/PhysRevE.76.031105 (2007).
13. Kaneyasu, M. & Hasegawa, Y. Quantum otto cycle under strong coupling. *Phys. Rev. E* **107**, 044127. https://doi.org/10.1103/PhysRevE.107.044127 (2023).
14. Mehta, V. & Johal, R. S. Quantum otto engine with exchange coupling in the presence of level degeneracy. *Phys. Rev. E* **96**, 032110. https://doi.org/10.1103/PhysRevE.96.032110 (2017).
15. Purkait, C. & Biswas, A. Measurement-based quantum otto engine with a two-spin system coupled by anisotropic interaction: Enhanced efficiency at finite times. *Phys. Rev. E* **107**, 054110. https://doi.org/10.1103/PhysRevE.107.054110 (2023).
16. Ishizaki, M., Hatano, N. & Tajima, H. Switching the function of the quantum otto cycle in non-markovian dynamics: Heat engine, heater, and heat pump. *Phys. Rev. Res.* **5**, 023066. https://doi.org/10.1103/PhysRevResearch.5.023066 (2023).
17. Cherubim, C., de Oliveira, T. R. & Jonathan, D. Nonadiabatic coupled-qubit otto cycle with bidirectional operation and efficiency gains. *Phys. Rev. E* **105**, 044120. https://doi.org/10.1103/PhysRevE.105.044120 (2022).
18. Son, J., Talkner, P. & Thingna, J. Monitoring quantum otto engines. *PRX Quantum* **2**, 040328. https://doi.org/10.1103/PRXQuantum.2.040328 (2021).
19. Singh, V. & Müstecaplıoğlu, O. E. Performance bounds of nonadiabatic quantum harmonic otto engine and refrigerator under a squeezed thermal reservoir. *Phys. Rev. E* **102**, 062123. https://doi.org/10.1103/PhysRevE.102.062123 (2020).
20. Chen, J.-F., Sun, C.-P. & Dong, H. Achieve higher efficiency at maximum power with finite-time quantum otto cycle. *Phys. Rev. E* **100**, 062140. https://doi.org/10.1103/PhysRevE.100.062140 (2019).
21. Leggio, B. & Antezza, M. Otto engine beyond its standard quantum limit. *Phys. Rev. E* **93**, 022122. https://doi.org/10.1103/PhysRevE.93.022122 (2016).
22. Huang, R., Xia, Y.-J. & Man, Z.-X. Manipulation and enhancement of the performance of otto cycle in the presence of nonthermal reservoirs. *New J. Phys.* **26**, 033052. https://doi.org/10.1088/1367-2630/ad3573 (2024).
23. Molitor, O. A. D. & Landi, G. T. Stroboscopic two-stroke quantum heat engines. *Phys. Rev. A* **102**, 042217. https://doi.org/10.1103/PhysRevA.102.042217 (2020).
24. Melo, F. V. et al. Implementation of a two-stroke quantum heat engine with a collisional model. *Phys. Rev. A* **106**, 032410. https://doi.org/10.1103/PhysRevA.106.032410 (2022).
25. Linden, N., Popescu, S. & Skrzypczyk, P. How small can thermal machines be? The smallest possible refrigerator. *Phys. Rev. Lett.* **105**, 130401. https://doi.org/10.1103/PhysRevLett.105.130401 (2010).
26. Müller, M. P. Correlating thermal machines and the second law at the nanoscale. *Phys. Rev. X* **8**, 041051. https://doi.org/10.1103/PhysRevX.8.041051 (2018).
27. Clivaz, F. et al. Unifying paradigms of quantum refrigeration: A universal and attainable bound on cooling. *Phys. Rev. Lett.* **123**, 170605. https://doi.org/10.1103/PhysRevLett.123.170605 (2019).
28. Brunner, N. et al. Entanglement enhances cooling in microscopic quantum refrigerators. *Phys. Rev. E* **89**, 032115. https://doi.org/10.1103/PhysRevE.89.032115 (2014).
29. Hewgill, A., Ferraro, A. & De Chiara, G. Quantum correlations and thermodynamic performances of two-qubit engines with local and common baths. *Phys. Rev. A* **98**, 042102. https://doi.org/10.1103/PhysRevA.98.042102 (2018).
30. Camati, P. A., Santos, J. F. G. & Serra, R. M. Coherence effects in the performance of the quantum otto heat engine. *Phys. Rev. A* **99**, 062103. https://doi.org/10.1103/PhysRevA.99.062103 (2019).

31. Uzdin, R., Levy, A. & Kosloff, R. Equivalence of quantum heat machines, and quantum-thermodynamic signatures. *Phys. Rev. X* **5**, 031044. https://doi.org/10.1103/PhysRevX.5.031044 (2015).
32. Peterson, J. P. S. et al. Experimental characterization of a spin quantum heat engine. *Phys. Rev. Lett.* **123**, 240601. https://doi.org/10.1103/PhysRevLett.123.240601 (2019).
33. Barrios, G. A., Albarrán-Arriagada, F., Cárdenas-López, F. A., Romero, G. & Retamal, J. C. Role of quantum correlations in light-matter quantum heat engines. *Phys. Rev. A* **96**, 052119. https://doi.org/10.1103/PhysRevA.96.052119 (2017).
34. Dillenschneider, R. & Lutz, E. Energetics of quantum correlations. *EPL (Europhysics Letters)* **88**, 50003 (2009).
35. Park, J. J., Kim, K.-H., Sagawa, T. & Kim, S. W. Heat engine driven by purely quantum information. *Phys. Rev. Lett.* **111**, 230402 (2013).
36. Brandner, K., Bauer, M., Schmid, M. T. & Seifert, U. Coherence-enhanced efficiency of feedback-driven quantum engines. *New J. Phys.* **17**, 065006 (2015).
37. Rahav, S., Harbola, U. & Mukamel, S. Heat fluctuations and coherences in a quantum heat engine. *Phys. Rev. A* **86**, 043843 (2012).
38. Uzdin, R. Coherence-induced reversibility and collective operation of quantum heat machines via coherence recycling. *Phys. Rev. Appl.* **6**, 024004 (2016).
39. Dorfman, K. E., Xu, D. & Cao, J. Efficiency at maximum power of a laser quantum heat engine enhanced by noise-induced coherence. *Phys. Rev. E* **97**, 042120. https://doi.org/10.1103/PhysRevE.97.042120 (2018).
40. Doyeux, P., Leggio, B., Messina, R. & Antezza, M. Quantum thermal machine acting on a many-body quantum system: Role of correlations in thermodynamic tasks. *Phys. Rev. E* **93**, 022134 (2016).
41. Klatzow, J. et al. Experimental demonstration of quantum effects in the operation of microscopic heat engines. *Phys. Rev. Lett.* **122**, 110601. https://doi.org/10.1103/PhysRevLett.122.110601 (2019).
42. Chiara, G. D. et al. Reconciliation of quantum local master equations with thermodynamics. *New J. Phys.* **20**, 113024. https://doi.org/10.1088/1367-2630/aaecee (2018).
43. Brask, J. B., Haack, G., Brunner, N. & Huber, M. Autonomous quantum thermal machine for generating steady-state entanglement. *New J. Phys.* **17**, 113029. https://doi.org/10.1088/1367-2630/17/11/113029 (2015).
44. Werlang, T., Marchiori, M. A., Cornelio, M. F. & Valente, D. Optimal rectification in the ultrastrong coupling regime. *Phys. Rev. E* **89**, 062109. https://doi.org/10.1103/PhysRevE.89.062109 (2014).
45. Man, Z.-X., An, N. B. & Xia, Y.-J. Controlling heat flows among three reservoirs asymmetrically coupled to two two-level systems. *Phys. Rev. E* **94**, 042135. https://doi.org/10.1103/PhysRevE.94.042135 (2016).
46. Hewgill, A., De Chiara, G. & Imparato, A. Quantum thermodynamically consistent local master equations. *Phys. Rev. Res.* **3**, 013165. https://doi.org/10.1103/PhysRevResearch.3.013165 (2021).
47. Landi, G. T., Poletti, D. & Schaller, G. Nonequilibrium boundary-driven quantum systems: Models, methods, and properties. *Rev. Mod. Phys.* **94**, 045006. https://doi.org/10.1103/RevModPhys.94.045006 (2022).
48. Man, Z.-X., Tavakoli, A., Brask, J. B. & Xia, Y.-J. Improving autonomous thermal entanglement generation using a common reservoir. *Phys. Scr.* **94**, 075101. https://doi.org/10.1088/1402-4896/ab0c51 (2019).
49. Manzano, G., Silva, R. & Parrondo, J. M. R. Autonomous thermal machine for amplification and control of energetic coherence. *Phys. Rev. E* **99**, 042135. https://doi.org/10.1103/PhysRevE.99.042135 (2019).
50. Hammam, K., Hassouni, Y., Fazio, R. & Manzano, G. Optimizing autonomous thermal machines powered by energetic coherence. *New J. Phys.* **23**, 043024. https://doi.org/10.1088/1367-2630/abeb47 (2021).
51. Wang, Y., Man, Z.-X., Zhang, Y.-J. & Xia, Y.-J. Work costs and operating regimes for different manners of system-reservoir interactions via collision model. *New J. Phys.* **24**, 053030. https://doi.org/10.1088/1367-2630/ac6a01 (2022).
52. Giovannetti, V. & Palma, G. M. Master equations for correlated quantum channels. *Phys. Rev. Lett.* **108**, 040401. https://doi.org/10.1103/PhysRevLett.108.040401 (2012).
53. Lorenzo, S., McCloskey, R., Ciccarello, F., Paternostro, M. & Palma, G. M. Landauer's principle in multipartite open quantum system dynamics. *Phys. Rev. Lett.* **115**, 120403. https://doi.org/10.1103/PhysRevLett.115.120403 (2015).
54. Lorenzo, S., Farace, A., Ciccarello, F., Palma, G. M. & Giovannetti, V. Heat flux and quantum correlations in dissipative cascaded systems. *Phys. Rev. A* **91**, 022121. https://doi.org/10.1103/PhysRevA.91.022121 (2015).
55. Zhang, Q., Xia, Y.-J. & Man, Z.-X. Effects of one-way correlations on thermodynamics of a multipartite open quantum system. *Phys. Rev. A* **108**, 062211. https://doi.org/10.1103/PhysRevA.108.062211 (2023).
56. Rau, J. Relaxation phenomena in spin and harmonic oscillator systems. *Phys. Rev.* **129**, 1880. https://doi.org/10.1103/PhysRev.129.1880 (1963).
57. Ciccarello, F., Lorenzo, S., Giovannetti, V. & Palma, G. M. Quantum collision models: Open system dynamics from repeated interactions. *Phys. Rep.* **954**, 1 (2022).
58. Man, Z.-X., Xia, Y.-J. & Lo Franco, R. Temperature effects on quantum non-markovianity via collision models. *Phys. Rev. A* **97**, 062104. https://doi.org/10.1103/PhysRevA.97.062104 (2018).
59. Jin, J. S. & s. Yu, C. Non-markovianity in the collision model with environmental block. *New J. Phys.* **20**, 053026 (2018). https://doi.org/10.1088/1367-2630/aac0cb.
60. Barra, F. The thermodynamic cost of driving quantum systems by their boundaries. *Sci. Rep.* **5**, 14873. https://doi.org/10.1038/srep14873 (2015).
61. Lorenzo, S., McCloskey, R., Ciccarello, F., Paternostro, M. & Palma, G. M. Landauer's principle in multipartite open quantum system dynamics. *Phys. Rev. Lett.* **115**, 120403. https://doi.org/10.1103/PhysRevLett.115.120403 (2015).
62. Pezzutto, M., Paternostro, M. & Omar, Y. Implications of non-markovian quantum dynamics for the landauer bound. *New J. Phys.* **18**, 123018. https://doi.org/10.1088/1367-2630/18/12/123018 (2016).
63. Man, Z.-X., Xia, Y.-J. & Lo Franco, R. Validity of the landauer principle and quantum memory effects via collisional models. *Phys. Rev. A* **99**, 042106. https://doi.org/10.1103/PhysRevA.99.042106 (2019).
64. Seah, S. et al. Collisional quantum thermometry. *Phys. Rev. Lett.* **123**, 180602. https://doi.org/10.1103/PhysRevLett.123.180602 (2019).
65. Buffoni, L., Solfanelli, A., Verrucchi, P., Cuccoli, A. & Campisi, M. Quantum measurement cooling. *Phys. Rev. Lett.* **122**, 070603. https://doi.org/10.1103/PhysRevLett.122.070603 (2019).

Acknowledgements

Author contributions

Z.X. and R.H. derived the theoretical results; R.H. and L. L. simulated the theoretical results; Z.X. wrote the main manuscript text. All authors reviewed the manuscript.

Declarations

Competing interests
The authors declare no competing interests.

Additional information
Correspondence and requests for materials should be addressed to Z.-X.M.

Reprints and permissions information is available at www.nature.com/reprints.

Publisher's note Springer Nature remains neutral with regard to jurisdictional claims in published maps and institutional affiliations.